Engineering Structures 318 (2024) 118711

Contents lists available at ScienceDirect

Engineering Structures

journal homepage: www.elsevier.com/locate/engstruct

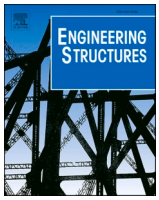

Quantification of shear transfer mechanisms in reinforced concrete deep beams using measured experimental data

Dhanushka K. Palipana [a], Alexandru N. Trandafir [b], Boyan I. Mihaylov [b], Giorgio T. Proestos [a,*]

[a] Department of Civil, Construction, and Environmental Engineering, North Carolina State University, 915 Partners Way, Raleigh, NC, 27695–7908, United States
[b] Department of ArGEnCo, University of Liege, Bât. B52/3, Quartier Polytech 1, Allée de la Découverte 9, 4000 Liège 1, Belgium

ARTICLE INFO

Keywords:
Reinforced concrete
Structures
Shear
Cracks
Deep beams
Assessment
Aggregate interlock

ABSTRACT

This paper presents a method to quantify the shear transfer mechanisms in large-scale, shear-critical, reinforced concrete deep beams from detailed experimental data. The results provide a fundamental understanding of structural behavior upon which direct crack-based assessment methods and improved modelling of crack interfaces can be developed. The Two-Parameter Kinematic Theory describes the behavior of deep beams subjected to shear and outlines a framework whereby shear is transferred through four mechanisms: by stresses in the uncracked region near the loading zone, through aggregate interlock, through the transverse reinforcement and through dowel action of the longitudinal reinforcement. This paper proposes an approach to directly quantify these shear transfer mechanisms by using measured data from large-scale experiments in conjunction with constitutive models. That is, the load on the structure can be assessed solely from the displacement field data and boundary conditions. The experimental data from six large-scale deep beams monitored with full field-of-view Digital Image Correlation (DIC) equipment throughout loading are examined. The paper demonstrates that the assessed load agrees well with the measured load from the experiments at the peak and throughout loading.

1. Introduction

Reinforced concrete structures, including buildings, bridges, offshore structures, storage silos, and nuclear containment structures, can exhibit cracks, either as a result of regular use or extreme events such as earthquakes. To delineate which structures require repair or retrofit and to determine the safety of cracked structures, methods are needed to better understand and interpret existing cracks in reinforced concrete members. Surface crack patterns and crack widths are often the only visual indicators of the condition of the concrete members being examined. Inspections to obtain crack patterns and crack width information are often conducted manually by inspectors. However, as technologies improve, Unmanned Vehicles (UVs) and image processing techniques [1,2] are also being used in field applications where manual inspections may be difficult.

Once crack measurements are obtained, safety assessments are conducted by comparing measured parameters with the allowable limits in guidance documents or predictions from models, such as finite element simulations. Direct crack-based assessment methods and other methodologies, such as machine learning approaches, are also being developed to quantify the safety of structures from crack information [3–6]. The development of crack-based assessment methods relies on a fundamental understanding of the load carrying mechanisms in the members and having reliable models to quantify each load carrying mechanism. Additionally, in scenarios where existing cracks or crack interfaces exist, establishing methods that can quantify the amount of shear transfer from measured data can be important to understanding the response of the member.

The assessment of shear transfer mechanisms from displacement field data has been examined by others for slender members [7]. However, a general method for the quantification of shear transfer mechanisms using detailed DIC data for deep beams has not been studied. Thus, this paper presents a new method to quantify the shear carrying mechanisms in large-scale deep concrete beams that can be used to inform how existing cracks transmit shear and how existing cracks contribute to member response. Specifically, this paper presents a method by which detailed displacement field data can be used to directly quantify the shear transmitted in shear critical reinforced concrete deep beams (see Fig. 1).

Reinforced concrete deep beams are structural elements with shear span-to-depth ratios (a/d) less than approximately 2.0 or 2.5. The response of deep beams is governed by shear deformations and

* Corresponding author.

https://doi.org/10.1016/j.engstruct.2024.118711
Received 31 March 2024; Received in revised form 21 June 2024; Accepted 25 July 2024
Available online 10 August 2024

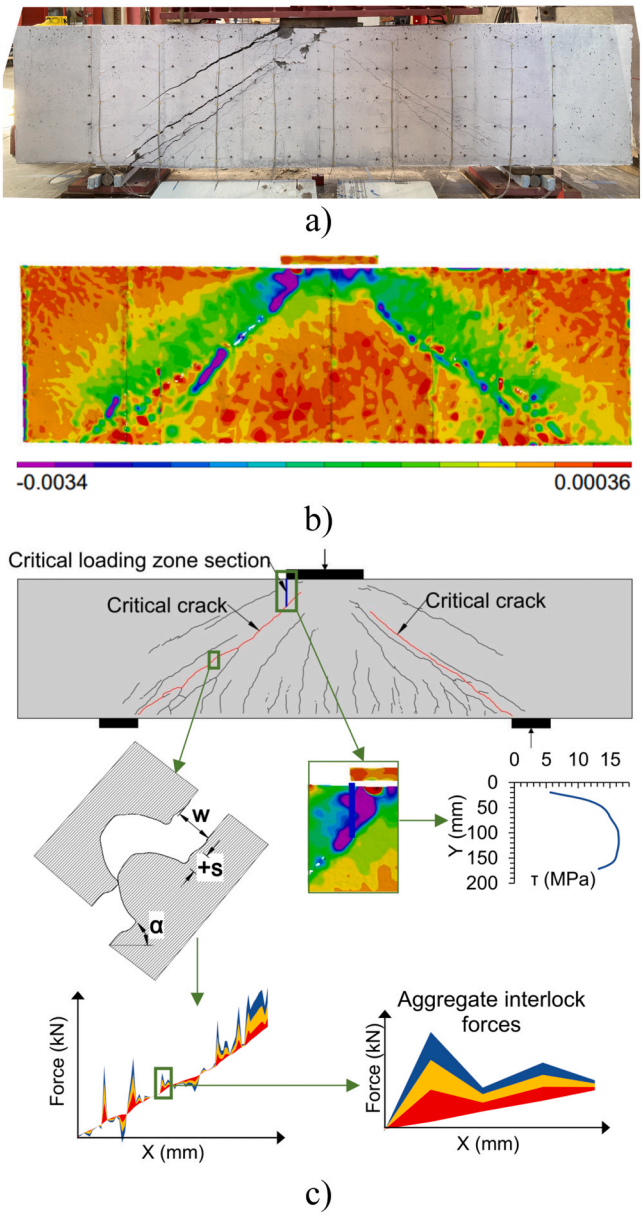

Fig. 1. a) A concrete deep beam after failure b) Principal compressive strains for a deep beam at the peak load obtained using full field-of-view DIC equipment c) Quantifying the shear transfer mechanisms using deformation data.

traditional methods, applicable to slender members, are insufficient to understand the full response of the members. Thus, more advanced methods, such as the Two-Parameter Kinematic Theory (2PKT) [8], capable of predicting the full response of deep beams subjected to shear, are needed. The 2PKT describes four transfer mechanisms by which deep beams can transmit shear: by the uncracked zone in compression, called the critical loading zone (V_{CLZ}), aggregate interlock (V_{ci}), transverse reinforcement (V_s), and dowel action (V_d). The summation of these mechanisms along a critical shear crack extending from the edge of the support plate to near the load gives the total shear carried by that shear span, as given in Eq. (1).

$$V = V_{CLZ} + V_{ci} + V_s + V_d \tag{1}$$

This paper presents an approach to quantify each of the four shear transfer mechanisms by using detailed, experimentally obtained, full field-of-view displacement field measurements as an input. The experimental data from a series of six large-scale deep beams are examined. Of the six monotonically loaded experiments, three are loaded symmetrically and three are loaded asymmetrically. The displacement fields of the specimens are monitored using full field-of-view Digital Image Correlation (DIC) equipment (see Fig. 1b). The measured deformation data are directly used in conjunction with constitutive models for each shear transfer mechanism to quantify them (see Fig. 1c). The quantified shear determined from the experimental data are compared to the applied shear for each shear span throughout loading. It should be emphasized that the proposed method is not a design method, but rather a new approach that can be used to gain insight into the load-carrying mechanisms in shear-critical deep beams. This insight can be used to improve crack-based assessment methods, design methods or inform codes and standards.

2. Summary of experiments examined

In this paper, experimental data from six large-scale deep beam experiments, called the CCR series, conducted at North Carolina State University and summarized in detail elsewhere, are studied [9–12]. The specimens measured 4877 mm long, 1105 mm deep, and 304.8 mm wide. The specimens had nine headed No. 9 bars for the bottom longitudinal reinforcement with an effective depth of 909 mm and two headed No. 9 bars for the top longitudinal reinforcement. No. 3 stirrups were spaced at 330 mm giving a transverse reinforcement ratio of 0.141 %. The properties of the reinforcement were determined from coupon tension tests. For the longitudinal reinforcement the Young's modulus (E_s) was 200 GPa, the yield stress (f_y) was 601 MPa, the ultimate stress (f_u) was 783 MPa, the strain-hardening strain (ε_{sh}) was 10.4×10^{-3}, and the ultimate strain (ε_u) was 110.4×10^{-3}. For the transverse reinforcement Young's modulus (E_s) was 200 GPa, the yield stress (f_y) was 494 MPa, the ultimate stress (f_u) was 759 MPa, the strain-hardening strain (ε_{sh}) was 9.0×10^{-3}, and the ultimate strain (ε_u) was 136.1×10^{-3}.

Specimens CCR1-CCR3 were symmetrically loaded with a point load in the center of the span of the member. These specimens had the same loading plate size (l_{b1}), but the shear span-to-depth ratios (a/d) varied. CCR4-CCR6 were asymmetrically loaded by offsetting the load from the center of the beam in two configurations. In CCR4 and CCR6, the load was applied 203 mm and 127 mm offset from the center of the symmetrically arranged loading plate. In CCR5, the load was applied at the center of the loading plate, which was offset 318 mm from the center of the beam. This resulted in different shear span-to-depth ratios on the two shear spans for CCR4-CCR6. Geometric and reinforcement details are shown in Fig. 2a. The specimens were simply supported and had support plates measuring 305 mm. The concrete strength (f'_c), l_{b1}, and a/d of the north and south shear spans are given in Table 1.

The specimens were monotonically loaded to failure. During loading, the full field-of-view displacement field of the specimens was monitored on the west face using three-dimensional Digital Image Correlation (DIC), see Fig. 2b. Throughout loading, load stages were conducted. At a load stage, the loading was paused, cracks were marked and measured using crack comparators, and high-resolution photos of the specimens were taken.

Initially, flexural cracks occurred at 226 kN - 380 kN. With increasing load, flexural cracks widened, and shear cracks formed. The shear cracks reached the mid-depth of the beams at 711 kN - 973 kN. With increasing load, the shear cracks extended and widened. Ultimately, all the specimens failed in shear. The peak load and failure span of each specimen are given in Table 1. Additional information on the experiments and a more detailed analysis of the experimental results can be found elsewhere in the literature [9–12].

Also shown in Table 1 are the peak strength predictions of the specimens using the ACI 318–19 Strut-and-Tie Method [13]. The specimens are lightly reinforced in the transverse direction and do not meet the minimum required (0.25 %) to satisfy the requirements for higher strut coefficients. The mean test-to-predicted ratio for the ACI 318–19

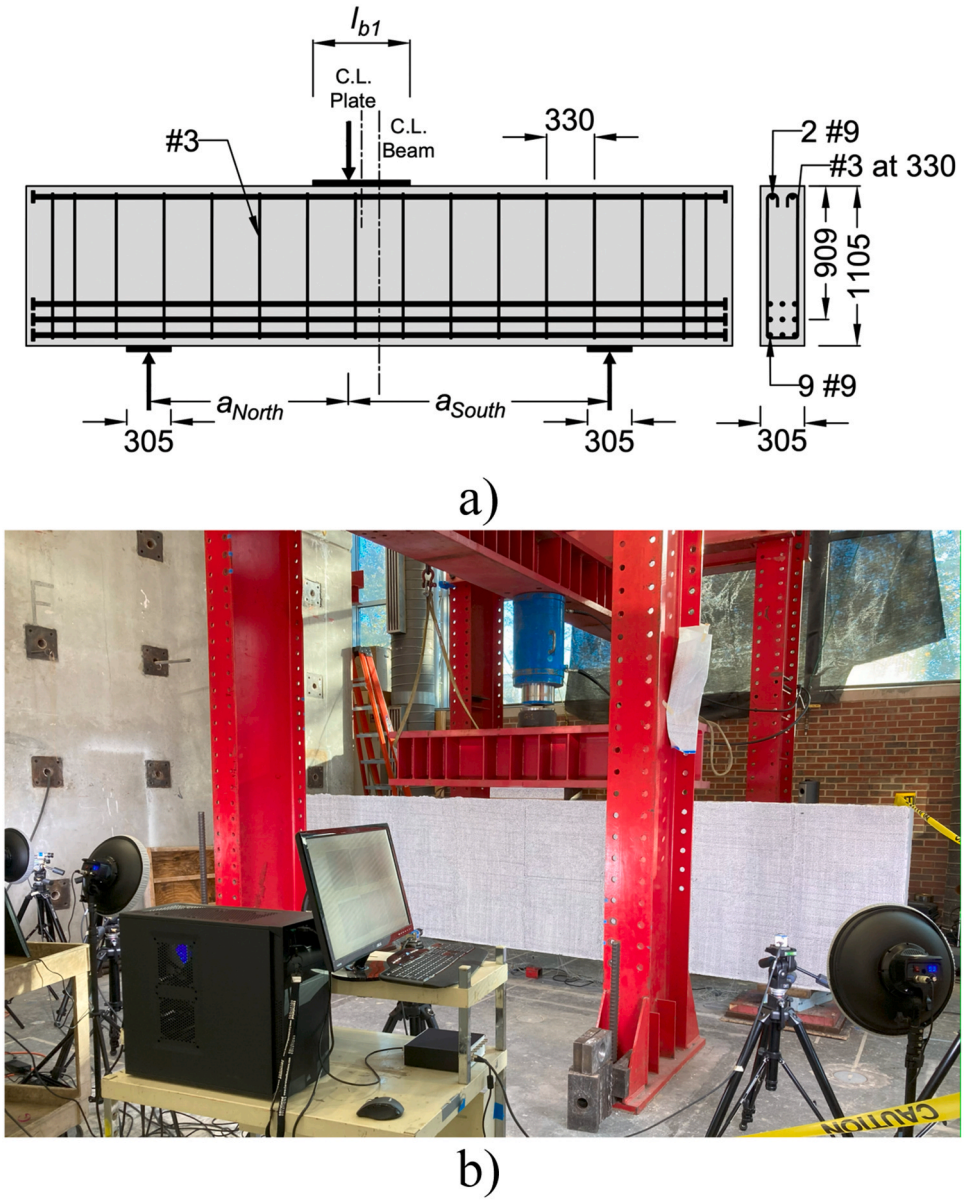

Fig. 2. a) Geometric and reinforcement details for CCR1-CCR6 (Note: All dimensions are in mm). b) Collecting deformation data using full field-of-view DIC on the west face of the specimens.

Table 1
Summary of CCR specimen details.

Specimen	f_c' (MPa)	a/d (North)	a/d (South)	a_{North} (mm)	a_{South} (mm)	l_{b1} (mm)	Peak shear of the failure span (kN)	Failure span	Loading configuration	$P_{ACI\ S\&T}$ (kN)	$\frac{P_{exp.}}{P_{ACI\ S\&T}}$
CCR1	34.5	2.25	2.25	2046	2046	610	958	South	Symmetrical loading	1197	1.60
CCR2	35.8	2.00	2.00	1819	1819	610	1118	North	Symmetrical loading	1404	1.59
CCR3	39.5	1.80	1.80	1637	1637	610	1307	South	Symmetrical loading	1723	1.52
CCR4	37.8	1.80	2.25	1637	2046	914	1296	North	Asymmetrical loading on a symmetrical loading plate	1428	1.63
CCR5	41.5	1.80	2.50	1637	2273	610	739	South	Symmetrical loading on an asymmetrical loading plate	1524	1.16
CCR6	39.3	2.11	2.39	1919	2173	914	964	North	Asymmetrical loading on a symmetrical loading plate	1378	1.32

Strut-and-Tie Nethod is 1.47 with a coefficient of variation of 13.0 %. This difference between the measured and predicted strengths is substantial and suggests that an improvement in the understanding of shear carrying mechanisms for deep beams, particularly those that are lightly reinforced, is needed. The balance of this paper aims to quantify the shear transfer mechanisms using measured deformation data obtained

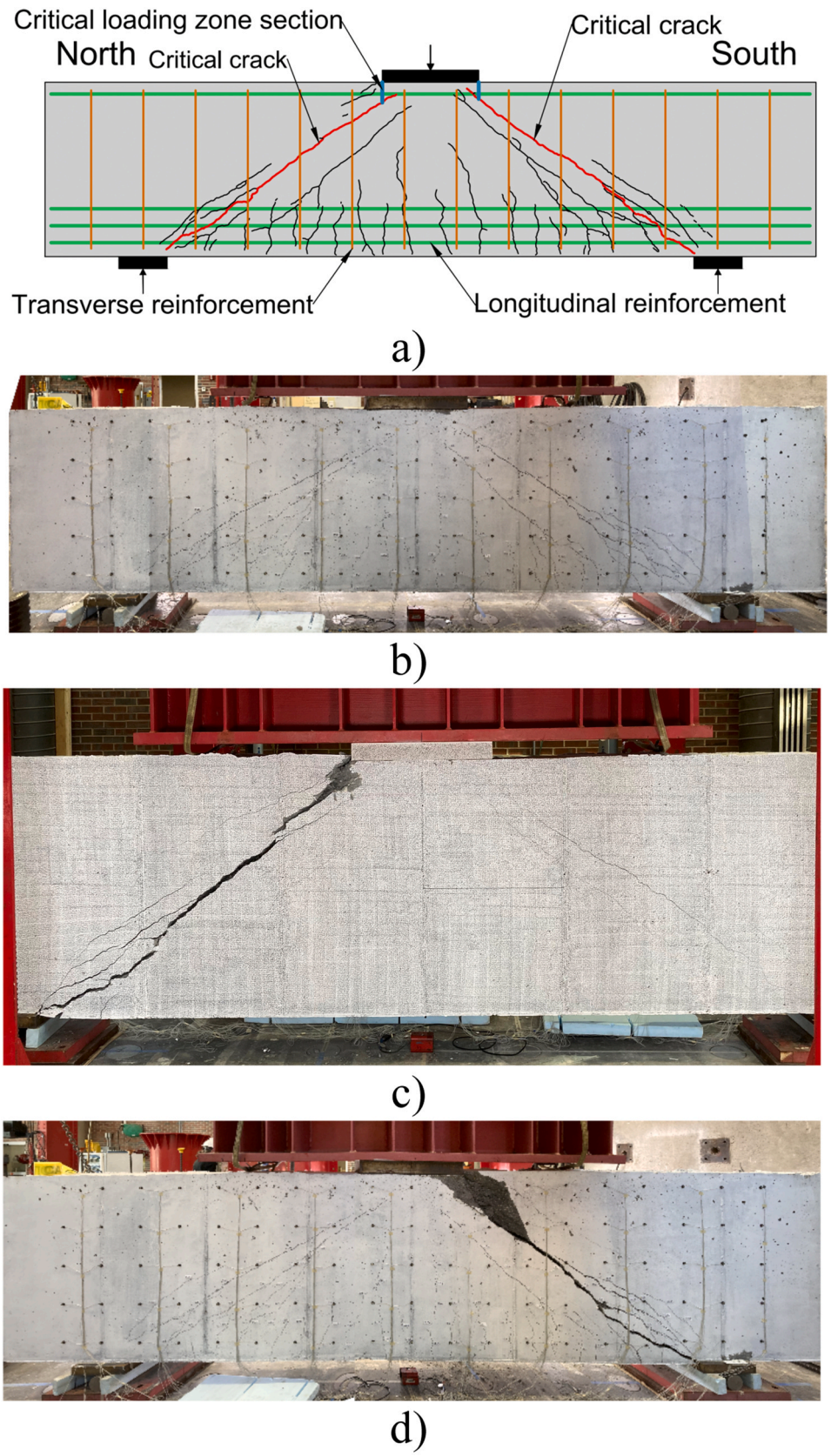

Fig. 3. a) The crack pattern obtained using the ACDM tool on the west face of CCR2, critical cracks (red), and vertical section in the CLZ (blue). b) East face at the last load stage of CCR2c) West face after failure of CCR2 d) East face after failure of CCR2.

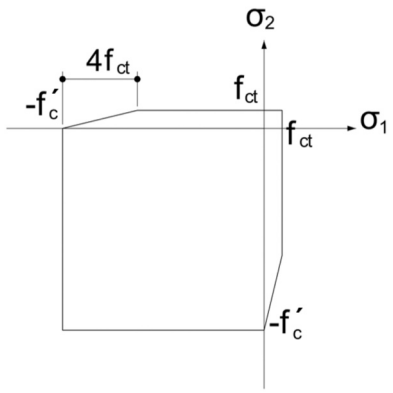

Fig. 4. Bilinear Kupfer biaxial failure criterion [18].

from the experiments. The improved understanding of the shear transfer mechanisms can be used to improve crack-based assessment techniques and design methods.

3. Shear transfer mechanisms in deep beams and their quantification using measured deformation data

This section describes how the shear transfer mechanisms in concrete deep beams can be directly quantified from experimentally obtained displacement field data. The 2PKT describes that deep beams transfer shear by four shear transfer mechanisms: by the uncracked zone in compression near the loading plate called the critical loading zone (V_{CLZ}), aggregate interlock (V_{ci}), transverse reinforcement (V_s), and dowel action (V_d). These four shear transfer mechanisms occur along a free body diagram extending from near the support plate, along the critical shear crack through the uncracked compression region up to the edge of the loading plate (see Fig. 3) [8].

The critical loading zone is the uncracked region in the vicinity of the loading plate that transmits shear in the compression region of the beam. Along critical shear cracks, aggregate interlock stresses develop and transmit shear stresses at the crack interface. Shear is also transmitted through transverse reinforcement that crosses the critical crack. The transverse displacements in the longitudinal reinforcement at the cracks results in shear transfer by dowel action. A more detailed explanation of the shear transfer mechanisms can be found elsewhere [3,8].

To conduct the quantification of the shear transmitted in the members, first, the crack patterns of the specimens at the peak load were generated using the Automated Crack Detection and Measurement (ACDM) tool [14]. This tool uses the principal tensile strain maps collected from the DIC data to identify cracked regions. The detected high-strain regions are thinned to obtain crack lines. The critical cracks in deep beams extend from near the inner edge of the support plate to near the edge of the loading plate and often exhibit the largest widths. The crack pattern generated for CCR2, and the critical cracks (red) are shown in Fig. 3a. The comparison of crack patterns shown in Fig. 3 demonstrates that this procedure gives reliable results for obtaining the detailed crack shape for the critical crack. A detailed discussion and additional verification and validation of generating crack patterns, comparing crack patterns on the east face with the west face of the specimens, obtaining crack displacement, and analyses can be found elsewhere [9–12].

In the 2PKT framework, to determine the shear force carried in a particular shear span, the equilibrium of a free body diagram (FBD) is considered. The FBD considered in this paper is determined by considering a vertical section at the edge of the loading plate up to its intersection with the critical crack. The vertical sections considered (one on each shear span) in the critical loading zone (CLZ) are shown for CCR2 in Fig. 3a (blue). Finally, the locations of transverse reinforcement and longitudinal reinforcement with respect to the crack pattern are identified (see Fig. 3a).

Once the crack patterns have been generated and the critical cracks, critical loading zone, and the locations of dowels and transverse reinforcement have been identified for each specimen, the four transfer mechanisms can be determined from the displacement field data as described below.

3.1. Critical loading zone

The critical loading zone is the highly compressed region near the edge of the loading plate [8]. Previous studies have shown that for deep beams, this mechanism can contribute up to 66 % of the total shear for similar, lightly reinforced deep beams [3].

The concrete compressive stresses in the CLZ are calculated using the Modified Popovics model in conjunction with the strains measured from the DIC data [15–17]. That is, the strain data from the DIC in the CLZ are used as inputs to the Modified Popovics model to determine the stresses in the CLZ in the principal compression direction, see Eqs. (2–5). Here, σ_2, f_c', ε_{cf}, ε_c' and E_c are the principal compressive stress, strength of concrete, measured strain, strain at uniaxial peak stress, and the modulus of elasticity of concrete, respectively. Predictions of the Modified Popovics model to concrete cylinder test data for these specimens were compared and agree well, see Palipana (2023) [9].

When $\varepsilon_{cf} < \varepsilon_c'$,

$$\sigma_2 = f_c' \frac{n\left(\frac{\varepsilon_{cf}}{\varepsilon_c'}\right)}{n-1+\left(\frac{\varepsilon_{cf}}{\varepsilon_c'}\right)^{nk}} \tag{2}$$

$$n = 0.8 + \frac{f_c'}{17} \tag{3}$$

$$\varepsilon_c' = \frac{f_c'}{E_c}\frac{n}{n-1} \tag{4}$$

$$if \frac{\varepsilon_{cf}}{\varepsilon_c'} < 1.0, \quad k = 1.0 \tag{5}$$

Otherwise,

$$\sigma_2 = f_c' \tag{6}$$

The post-peak compressive strength is approximated with a non-decaying plastic plateau in regions with high confinement, as shown in Eq. (6). This is appropriate because the concrete in the highly compressed region near the loading plate is biaxially confined. In other locations where tensile stresses occur, the tensile behavior of concrete is modeled as linear up to the cracking stress. The initial elastic modulus was taken to be $E_c = 1000(f_c')^{1/3}$ (MPa).

The interaction of biaxial stresses was modeled using Kupfer biaxial model [18]. This criterion for the combined tension-compression regime is simplified by assuming a bilinear law (see top-left and bottom right quadrants in Fig. 4). In Fig. 4, f_{ct} is the cracking stress which is taken equal to $0.33\sqrt{f_c'}$ (MPa).

To obtain the principal stresses for a particular point in the CLZ, the principal strains obtained from the DIC data are used as input into the Modified Popovics stress-strain relationships and the bilinear Kupfer biaxial failure criterion to obtain principal stresses. Here, it is assumed that the principal stress direction is coincident with the principal strain direction.

Fig. 5 shows the principal compressive strain plot obtained for CCR1 at the peak load. The light blue regions show the post-peak strains calculated using the DIC data in conjunction with the Modified Popovics relationship and the Kupfer biaxial failure criterion. Therefore, the light blue region shows the highly compressed regions of the specimen at the peak load.

To determine the total shear transmitted in the critical loading zone,

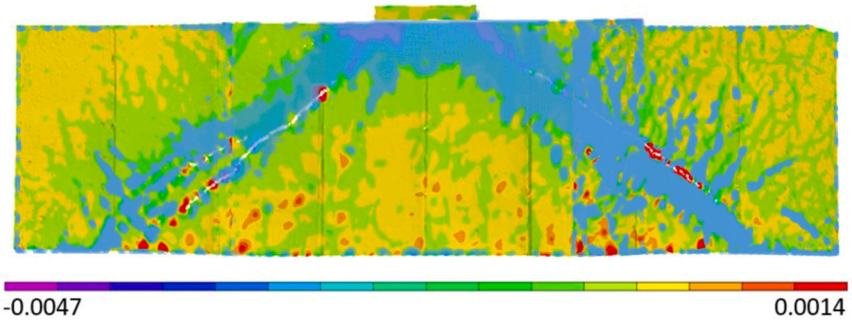

Fig. 5. Principal compressive strains (ε_2) in CCR1 at the peak load.

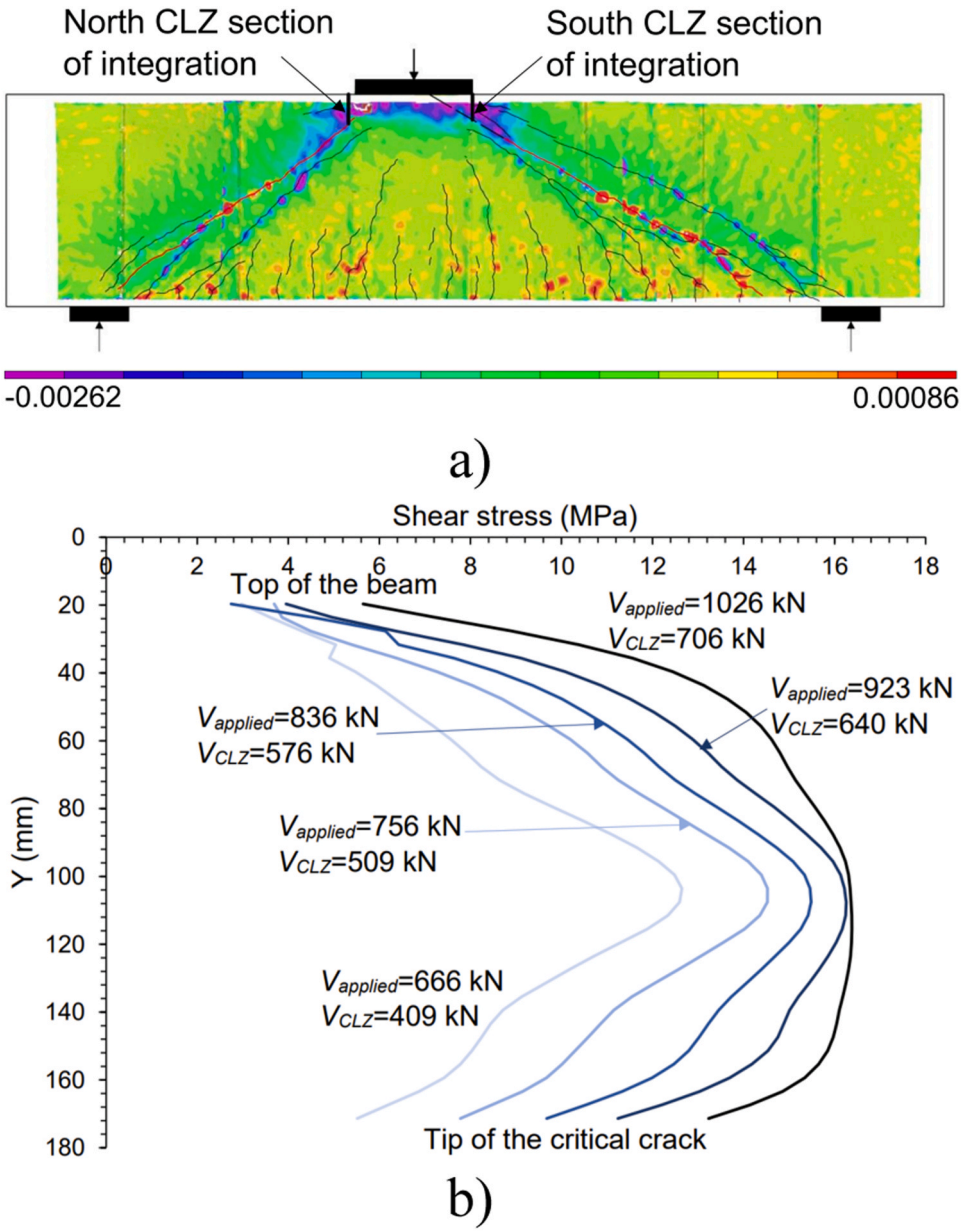

Fig. 6. a) Principal compressive strains and the vertical sections in CLZ for CCR5 b) the shear stresses at the critical loading zone (CLZ) section for north shear span of CCR5.

Table 2
Summary of quantified shear transfer mechanisms.

Specimen	Span	Failure span	$V_{app.}$ (kN)	$P_{app.}$ (kN)	V_{CLZ} (kN)	V_{ci} (kN)	V_s (kN)	V_d (kN)	$V_{ass.}$ (kN)	$P_{ass.}$ (kN)	$\frac{V_{app.}}{V_{ass.}}$	$\frac{P_{app.}}{P_{ass.}}$
CCR1	North		958	1916	457	160	357	54	1028	1827	0.93	1.05
	South	Failure	958		156	178	434	31	799		1.20	
CCR2	North	Failure	1106	2212	618	166	385	19	1188	2086	0.93	1.06
	South		1106		390	160	342	6	898		1.23	
CCR3	North		1307	2614	854	64	257	23	1199	2234	1.09	1.17
	South	Failure	1307		697	75	247	16	1035		1.26	
CCR4	North	Failure	1296	2333	622	18	311	21	968	2195	1.33	1.06
	South		1037		752	138	323	14	1227		0.85	
CCR5	North		1026	1765	706	62	300	26	1094	1921	0.94	0.92
	South	Failure	739		385	103	325	14	827		0.89	
CCR6	North	Failure	964	1816	730	87	258	17	1092	1953	0.88	0.93
	South		852		444	91	316	10	861		0.99	
										Avg	1.04	1.03
										COV	16.4 %	9.1 %

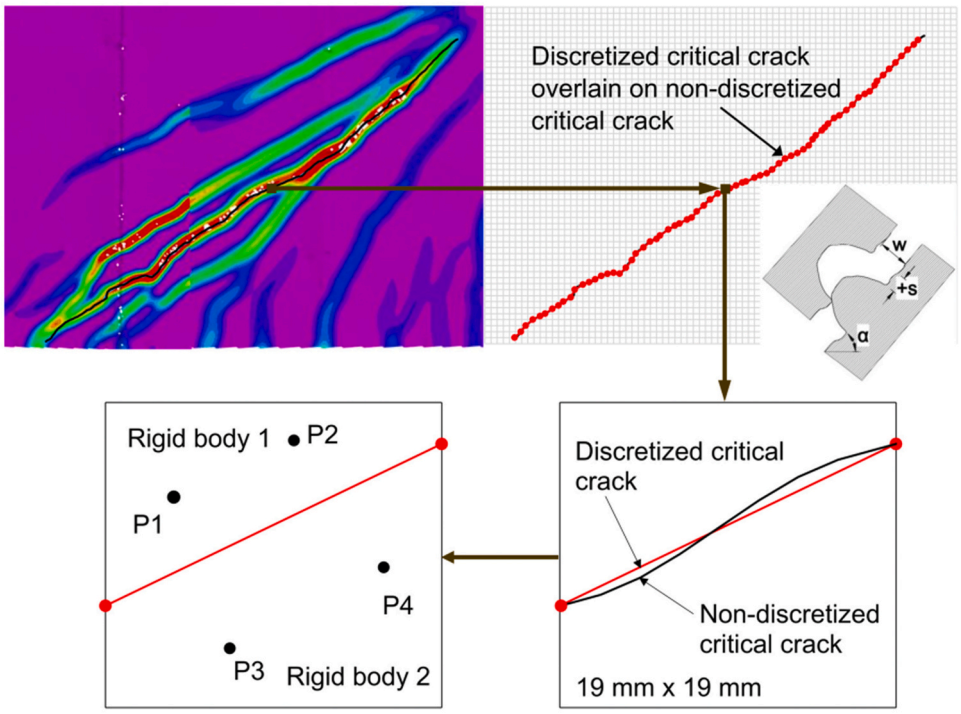

Fig. 7. Determining crack widths and crack slips (North shear span of CCR3).

a vertical section from the edge of the loading plate to the intersection point of the critical crack was considered (see Fig. 6a). Using tensor transformations, the principal stresses are converted to shear stresses along the vertical section. Fig. 6b shows the shear stresses in the CLZ obtained for the north shear span of CCR5 at several shear forces. The vertical shear stresses were integrated along the section and multiplied by the beam width to obtain shear force transmitted in the critical loading zone, V_{CLZ}. The quantified V_{CLZ} at the peak load is shown in Table 2.

3.2. Aggregate interlock

Aggregate interlock occurs when the opposite surfaces of a crack interface displace relative to each other. The relative displacements of one crack surface perpendicular to the other crack surface are called the crack widths (w), while the relative displacements parallel to the crack surface are called the crack slips (s), see Fig. 7. Previous studies have shown that for similar deep beams, this shear carrying mechanism can contribute up to 24 % of the shear transfer in lightly reinforced members [3]. Crack widths and crack slips can be used to quantify shear transfer by aggregate interlock using aggregate interlock models [3,19–21].

To quantify the amount of shear transmitted through aggregate interlock, the identified critical crack on each shear span of the specimens was divided into smaller crack segments using a grid equal to the maximum coarse aggregate size of 19 mm, see Fig. 7. This scale of discretization is based on previous research related to crack-based assessment of reinforced concrete deep beams [4].

For each crack segment (red lines in Fig. 7), a rigid body is defined on either side of the crack. Using the DIC measured displacement field, the crack kinematics of each crack segment were calculated. As shown in Fig. 7, the displacements of Rigid body 1 are defined by the points P1 and P2 and the displacements of Rigid body 2 are defined by points P3 and P4. The points are selected approximately 5–40 mm away from the crack edge to avoid spurious displacement field data at the crack. Additionally, the points were selected to so that the displacements of adjacent cracks were not incorporated into the measurements. Using

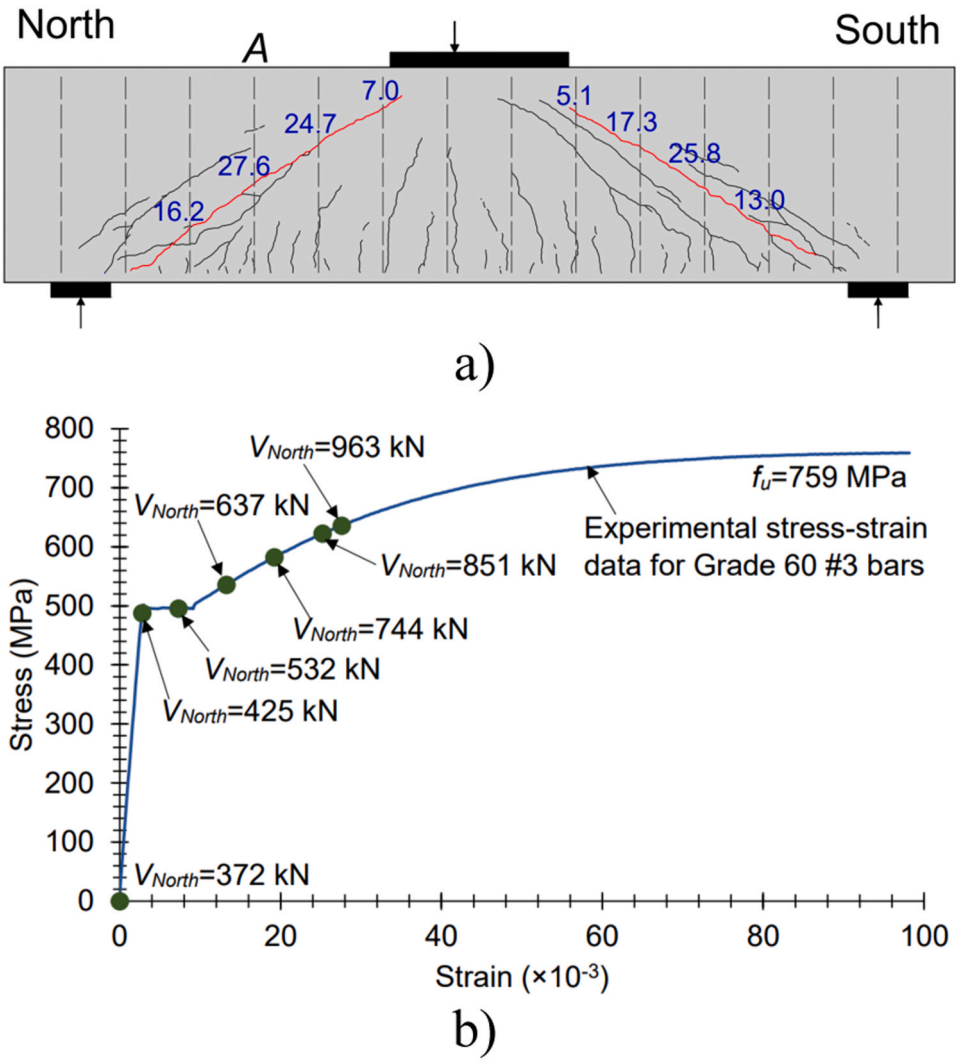

Fig. 8. a) Reinforcement strains calculated for CCR6 at the peak load (x10^{-3}). b) State of stress variation with the shear force for stirrup 'A' in the north shear span of CCR6.

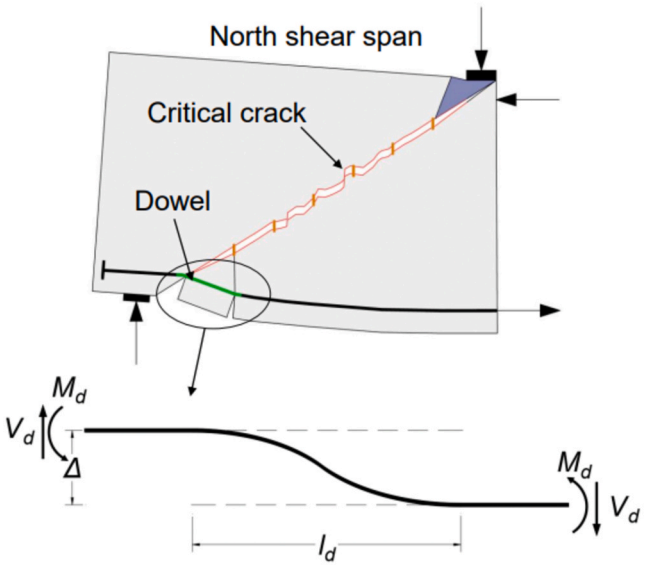

Fig. 9. Dowel action mechanism in a deep beam.

these points, the relative translation in two orthogonal directions and rotation of the rigid bodies can be determined. Using the angle of the crack segment with these two translations and one rotation, the crack widths, the crack slips, the vertical crack displacements and the horizontal crack displacements can be determined. A more detailed explanation of obtaining the crack kinematics is given in Palipana et al. (2022) [3].

These crack widths and crack slips were determined for each crack segment throughout loading. The aggregate interlock stress on each crack segment were then determined from the Modified Contact Density Model (CDM) using the crack widths and slips measured from the DIC data [22].

Specifically, using the CDM, the tangential (τ) and normal (σ) stresses at the crack surface can be calculated using the crack width (w), crack slip (s), concrete strength (f_c'), and maximum coarse aggregate size (a_g). See Eqs. (7) and (8). The angle θ is the direction of the small contact units which idealize the crack surface. The contact density function, $\Omega(\theta)$, represents the area of a contact unit and is approximated by the trigonometric cosine function, $0.5\cos\theta$. The surface area per unit crack plane, A_t, was calculated using the contact density function as a constant 1.27. The compressive stress on a contact unit, $\sigma_{con}(\theta)$, is obtained by assuming an elastic perfectly plastic behavior. To adapt the CDM for large-scale shear critical members that exhibit large crack widths and slips, a reduction factor of 0.35 was applied on $\sigma_{con}(\theta)$. This modification

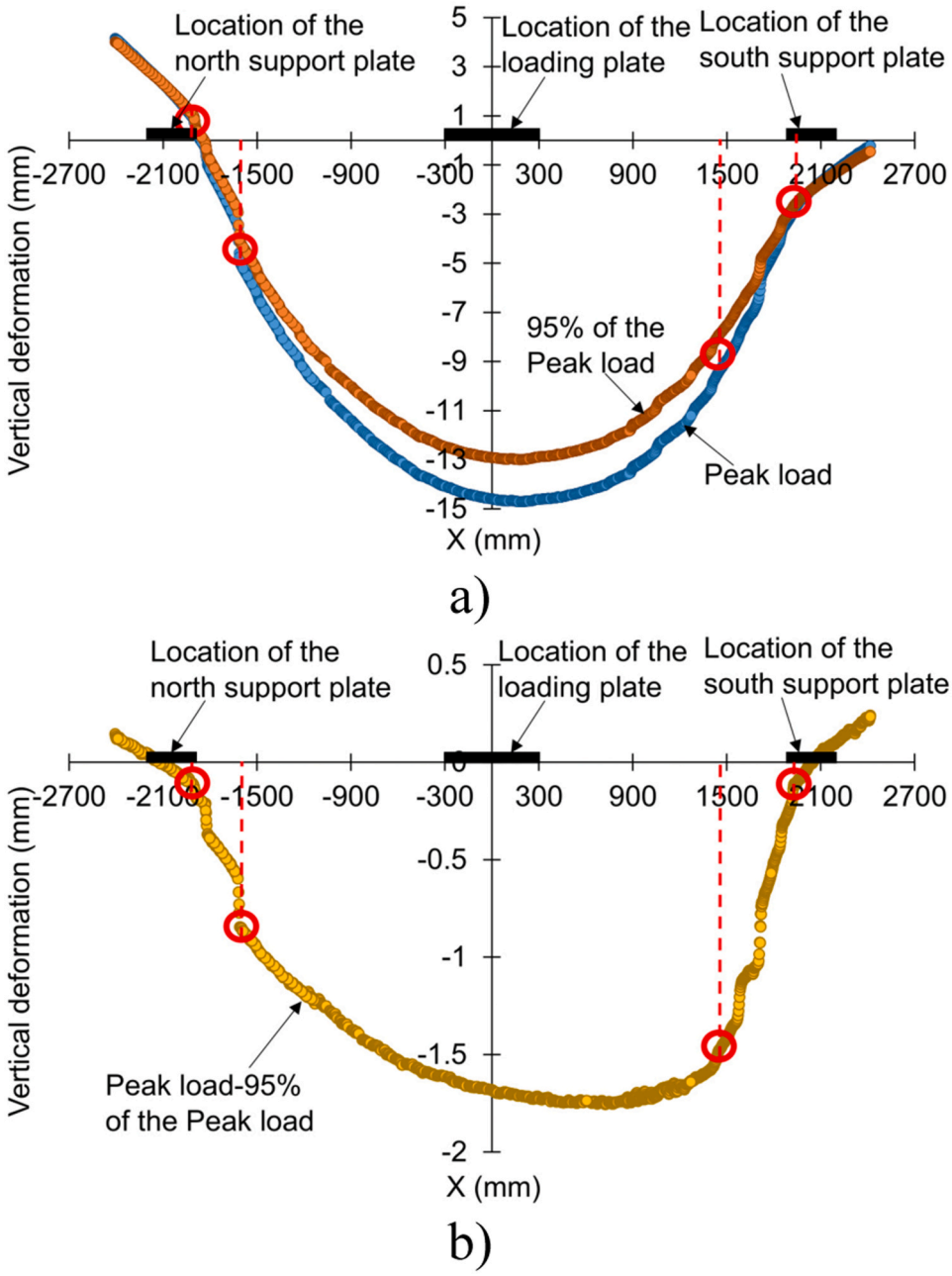

Fig. 10. a) Vertical deformations along the bottom-most longitudinal reinforcement bar of CCR1 at 95 % and 100 % of peak load, b) Incremental vertical deformation between 95 % and 100 % of peak load.

is explained and validated elsewhere [3,4].

$$\tau = \int_{-\pi/2}^{\pi/2} A_t \quad \sigma_{con}(\theta) K(w) \Omega(\theta) \sin\theta d\theta \tag{7}$$

$$\sigma = \int_{-\pi/2}^{\pi/2} A_t \quad \sigma_{con}(\theta) \quad K(w) \Omega(\theta) \cos\theta d\theta \tag{8}$$

Function $K(w)$, which accounts for the gradual loss of contact between the crack faces as the crack widths increase, is given by Eq. (9).

$$K(w) = 1 - \exp\left(1 - \frac{0.5 a_g}{w}\right) \geq 0 \tag{9}$$

Thus, the tangential and normal stresses along each crack segment can be determined from the crack widths and slips. These stresses are multiplied by the cross-sectional area of the crack segment to calculate the aggregate interlock force for that crack segment. Using the angle of the crack segment (α_i) with respect to the horizontal axis of the member, the vertical component of the forces is determined. These forces are then summed for all crack segments, see Eq. (10). The contribution of each crack segment up to the intersection point of the critical crack and the vertical section is summed to obtain the total shear force transmitted by aggregate interlock, V_{ci}. The calculated quantity of V_{ci} for each specimen and shear span are shown in Table 2.

$$V_{ci} = \sum_{i=1}^{n} [(\tau_i \bullet \sin\alpha_i - \sigma_i \bullet \cos\alpha_i) \bullet l_i \bullet b] \tag{10}$$

3.3. Transverse reinforcement

The transverse reinforcement that crosses the critical crack also contributes to the total amount of shear that can be transmitted in the

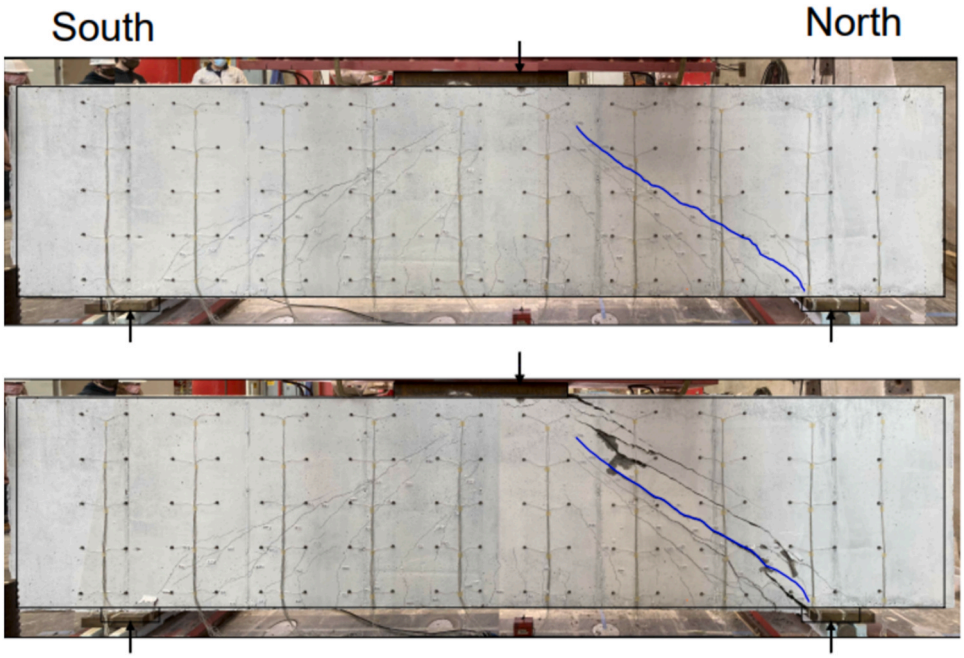

Fig. 11. CCR4 on the east side at the last load stage (top) and after failure (bottom).

specimens. Previous studies on deep beams with similar quantities of reinforcement have shown that this mechanism can contribute up to 46 % of the shear, even in lightly reinforced members [3]. The amount of force resisted by the transverse reinforcement across the critical crack is a function of the strain in the reinforcement. To quantify the amount of shear transmitted in the shear reinforcement, the DIC deformation data was used to determine the strain in each transverse reinforcing bar that crosses the critical crack. The difference in displacement measurements were determined over an estimated unbonded length and the average engineering strain over the unbonded length was determined (additional details on are discussed below). These strains were then used in conjunction with the stress-strain response of the steel to determine the stress in each reinforcing bar. The forces in each bar were then calculated and summed to determine the total shear transmitted by the transverse reinforcement, V_s.

To determine the strains in the reinforcement from DIC data an assumption is needed to convert surface displacements to reinforcement displacements. To convert the surface displacement data to average bar strain, an effective unbonded length can be used. That is, over the unbonded length the strains in the transverse bars are constant. The Maekawa et al. (2003) bond model is used as the basis to determine the strain in the reinforcement [22]. When a crack forms across reinforcement, in the vicinity of the crack, the reinforcing bar becomes debonded with the concrete. The Maekeawa et al. (2003) bond model proposes that the bond stress is deteriorated over a distance of 5D from the crack, where D is the diameter of the bar. Therefore, to determine the strains in the reinforcing bars from the DIC data, an unbonded length equal to 10D is used (5D on either side of the crack). In some scenarios cracks may be spaced closer than 10D. In these cases, the spacing between the two adjacent cracks was used as the unbonded length, as it is reasonable to assume that the transverse bar is unbonded over this length. Thus, the unbonded length considered is the lesser of 10D and the crack spacing at the intersection point of the critical crack. As an example, the calculated strains at the peak load for CCR6 are shown in Fig. 8a.

The strains calculated using DIC measurements were used to obtain the stresses in each bar from the experimentally obtained stress-strain behavior of the transverse reinforcement (see Fig. 8b). The green circles in Fig. 8b show the stress state of stirrup 'A' for varying shear forces in the north shear span of CCR6. Except for some stirrups near the edge of the support plates, all the stirrups in the six specimens tested reached the yield strain at the peak load.

3.4. Dowel action

Dowel action is the shear carried by the longitudinal bars resisting transverse displacements. Previous studies have shown that for deep beams with similar detailing and reinforcement quantities, this mechanism can contribute up to 9 % of the shear transfer [3]. The contribution of dowel action can be calculated by assuming the longitudinal bars crossing the critical crack acts as a flexural element in symmetrical double curvature (see Fig. 9). Thus, the relative transverse displacement between the ends of the dowel, Δ, the dowel length, l_d, the number of bars in each layer of reinforcement, n_b, and the moment of inertia of a single bar, I_b can be used to determine the dowel action V_d using Eqs. (11–13).

$$V_d = \frac{12E_sI_b}{l_d^3} n_b \Delta \leq V_{d,\max} \tag{11}$$

$$V_{d,\max} = n_b f_{y,eff} \frac{d_b^3}{3l_d} \tag{12}$$

$$f_{y,eff} = f_y \left[1 - \left(\frac{\varepsilon_{t,avg}}{\varepsilon_y} \right)^2 \right] \geq 0 \tag{13}$$

DIC data was used to obtain the deformation of the longitudinal bars throughout loading. Near the peak load, a large part of the deformations is caused by deformations at the critical crack. Therefore, to determine the length and the vertical displacement of the dowels, a comparison is made between vertical deformations along the bar at peak load and at 95 % of the peak load. Fig. 10 shows the vertical deformations along the bottom-most longitudinal reinforcement bar for CCR1 at the peak load and at 95 % of the peak load. The bottom yellow curve shows the deformations at 95 % of the peak load deducted from the deformations at the peak load. As can be seen in Fig. 10b, the difference between these displacements shows a rapid increase in vertical deformations around the critical crack. There is no significant increase in the deformations between the shear cracks on the north and south shear spans. The identified hinge points are shown by the red circles in Fig. 10.

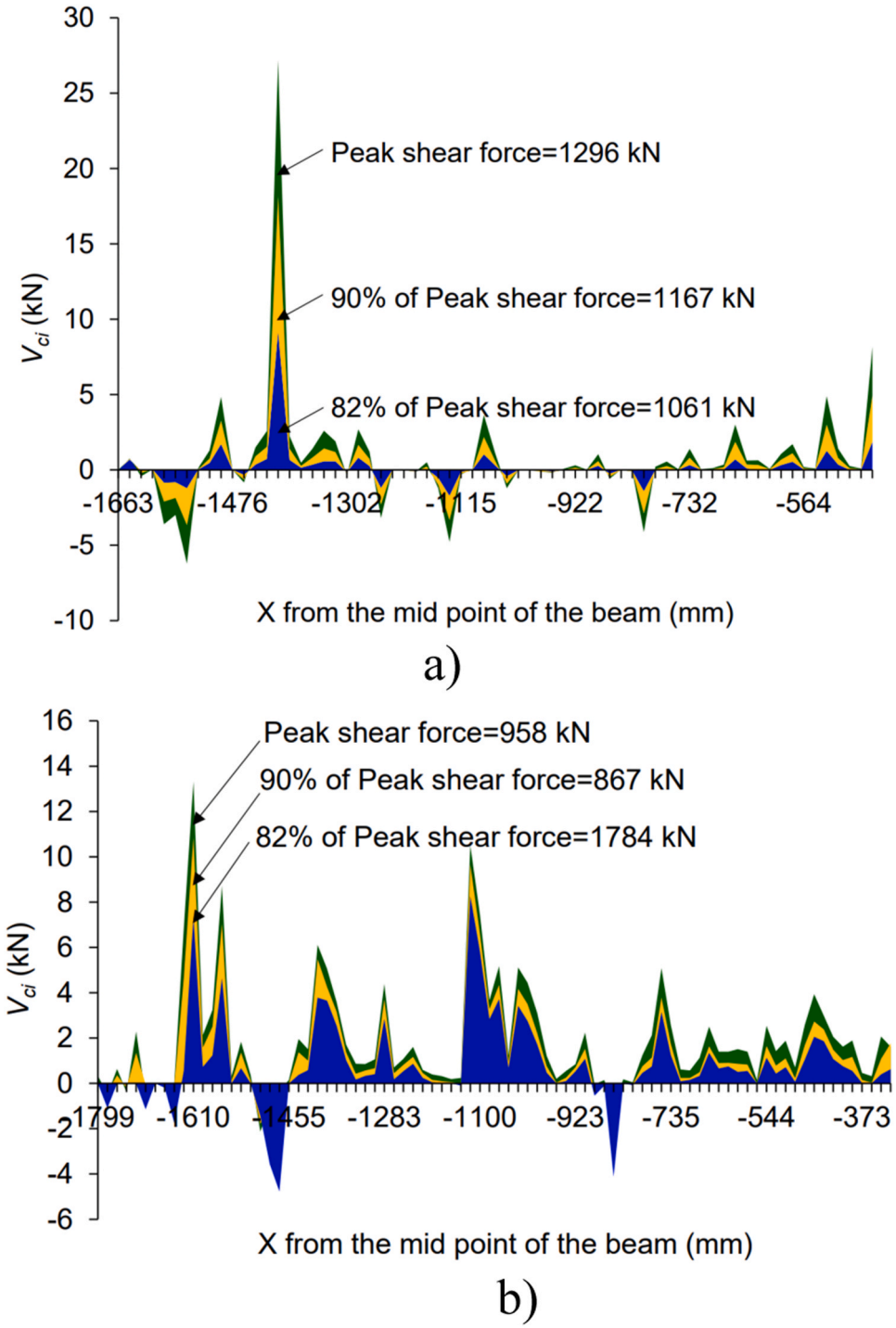

Fig. 12. Variation of V_{ci} along the north critical crack of: a) CCR4 and b) CCR1.

The distance between the hinge points is the dowel length, l_d. The analysis also shows that the length l_d remained approximately at the same location of the bar, throughout loading. The vertical and horizontal displacement were determined by examining the DIC measured displacement field over the dowel length, l_d. The vertical displacement between the ends of the dowel is the dowel deformation, Δ. The average axial strain in the dowel was calculated from the DIC displacement field data by determining the change in length of the dowel over the dowel length, l_d. For each layer of bottom longitudinal reinforcement, these parameters were input to Eqs. (11–13) and the dowel resistance for each layer of longitudinal reinforcement in the flexural tension region were summed to obtain the shear force transmitted by dowel action, V_d. The shear transmitted by dowel action calculated using this procedure is summarized in Table 2.

4. Results and discussion

A summary of the shear transfer mechanisms calculated at the peak load for both shear spans of the six specimens is given in Table 2. Note that, for CCR2, because of large amount of spalling at the peak load, the analysis was conducted at 99 % of the peak load. The four shear transfer mechanisms are summed to obtain the total assessed shear, $V_{ass.}$. The

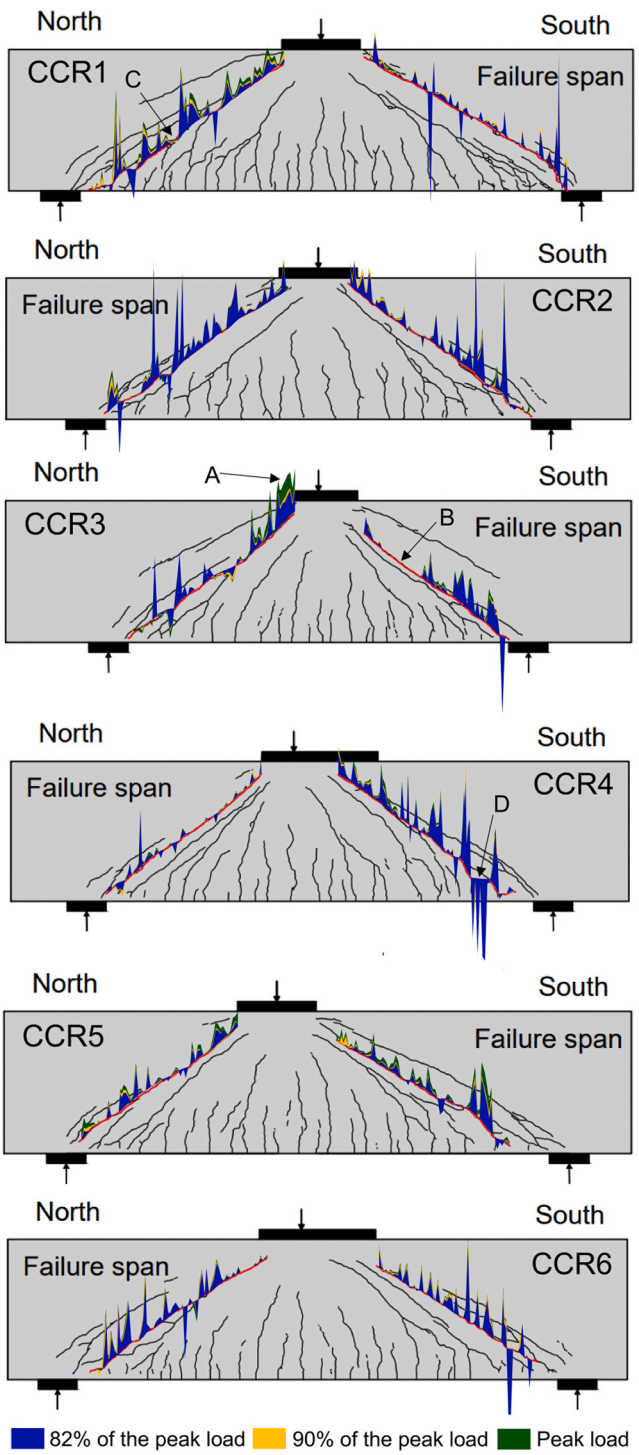

Fig. 13. Crack patterns and quantified aggregate interlock along the critical cracks for CCR1-CCR6 at the peak load.

assessed shear is compared with the applied shear, $V_{app.}$, measured in the experiment to evaluate the quality of the proposed approach for the quantification of shear transfer mechanisms in deep beams. The $V_{app.}/V_{ass.}$ ratios for both shear spans of all the specimens are shown in Table 2. The $V_{app.}/V_{ass.}$ ratios vary between 0.85 and 1.33. The average $V_{app.}/V_{ass.}$ is 1.04, and the coefficient of variation is 16.4 %. The table also shows the summation of the assessed shear transfer mechanisms of both shear spans and the assessed load, $P_{ass.}$. The assessed load is compared with the total applied load, $P_{app.}$. The $P_{app.}/P_{ass.}$ ratios are shown in Table 2. The $P_{app.}/P_{ass.}$ ratios vary between 0.92 and 1.17. The average $P_{app.}/P_{ass.}$ is 1.03, while the COV is 9.1 %. While the proposed quantification approach is not a design method, it should be noted that these results are obtained without the use of load factors or strength reduction factors. In practice, the assessment of structures should be conducted with consideration for margins of safety.

In the failure shear span, the difference in depth of the critical loading zones was compared for the east and west faces for each specimen. There was reasonable agreement except for the failure shear span of CCR4 where it was observed that the depth of the vertical section was 58 % larger on the east face of the specimen than the west face of the specimen. Fig. 11 shows the east face of CCR4 at last load stage and after failure. The blue line shows the critical crack on the north shear span. To account for this difference of the depths on the two faces, the V_{CLZ} was calculated by considering the average depth of CLZ on the east face and west face. The contribution for this mechanism was prorated to account for the average depth.

Except for the south shear span of CCR1, the CLZ provides the largest contribution to the total shear carrying mechanisms. When the symmetrically loaded specimens CCR1-CCR3, which have the same l_{b1} but different a/d ratios, are compared, there is an increase in V_{CLZ} with decreasing a/d, as is predicted by the 2PKT. The south shear span of CCR3 and north shear span of CCR4 had the same a/d ratio. However, the south shear span of CCR3 had 13 % larger V_{CLZ} than the north shear span of CCR4. Although CCR4 used a larger loading plate than CCR3, the asymmetric load has reduced the effective loading plate size on the north shear span of CCR4 resulting in a smaller V_{CLZ}. Comparing the north and the south shear spans of CCR1 shows how the crack geometry influences the amount of shear carried in the CLZ. For this specimen, the crack enters the region under the loading plate and results in a V_{CLZ} for the north shear span that is 2.93 times larger than V_{CLZ} of the south shear span, see Table 2. This is also true for CCR2 and CCR3, which shows V_{CLZ} for the north shear span is 1.58 and 1.23 times larger than V_{CLZ} on the south shear span, respectively.

The smallest V_{ci} is observed in the north shear span of CCR4. These small shear stresses are a result of small slips on the crack. Fig. 12a shows the variation of vertical component of aggregate interlock along the north critical crack of CCR4 at the peak shear force, 90 % of the peak shear force and 82 % of the peak shear force. As can be seen, the aggregate interlock forces remain small for the total shear forces shown. Fig. 12b shows the variation of the vertical component of aggregate interlock along the north critical crack of CCR1 at the peak shear force, 90 % of the peak shear force and 82 % of the peak shear force. For both shear spans shown, the shear force transmitted by aggregate interlock increases with the increase of the shear force on that shear span.

The largest V_{ci} is observed in the south shear span of CCR1. It was observed that the larger V_{ci} was a result of the larger slips on the crack. Fig. 13 illustrates the calculated vertical aggregate interlock force along the critical crack as a percentage of the total aggregate interlock for CCR1-CCR6. The red cracks are the critical cracks on each shear span. The height of the regions from the critical crack corresponds to the percentage of total aggregate interlock force carried by that crack segment at the peak load. It was observed that larger crack slips result in larger aggregate interlock forces, see point 'A', while smaller crack slips result smaller aggregate interlock forces, see point 'B'. The plots also show that large crack segment angles result in large aggregate interlock forces, while shallow crack segment angles result in small aggregate interlock forces. For example, 'C' in Fig. 13, has similar crack widths and crack slips, however, the increase of crack angle has resulted in larger aggregate interlock forces. When crack segments are nearly horizontal or have negative crack slips, these crack segments can have negative aggregate interlock forces. See point 'D' in Fig. 13.

The V_s component in specimens CCR1-CCR3 indicates that when the a/d ratio decreases, the amount of shear transmitted by V_s decreases, see Table 2. This is also true when the shear spans of asymmetrically loaded specimens CCR4-CCR6 are compared. This is a result of the critical crack crossing a smaller number of transverse reinforcing bars in the shorter

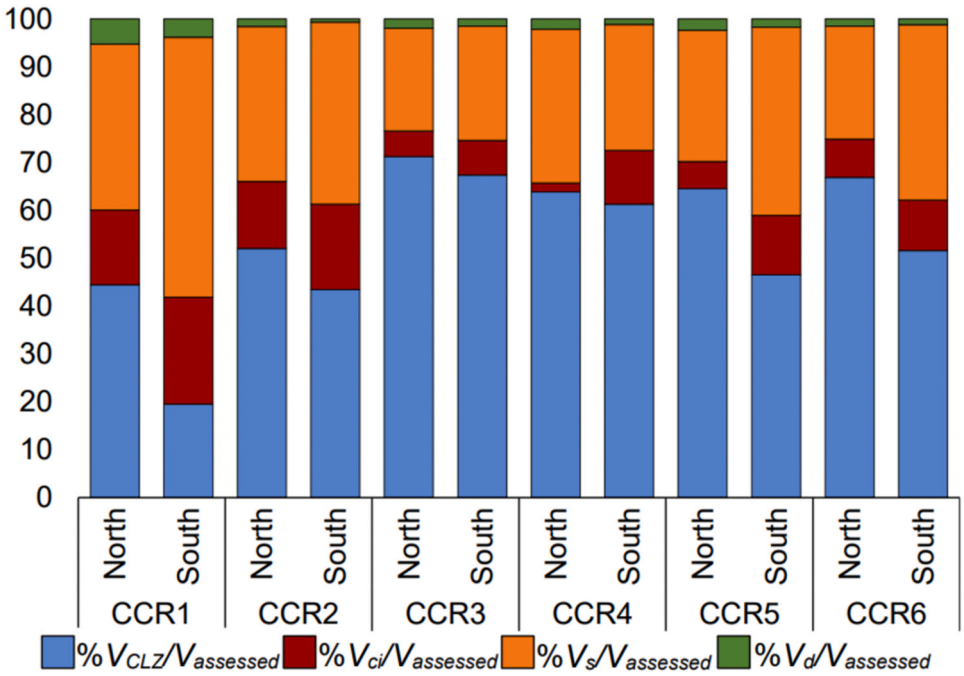

Fig. 14. Shear transfer mechanisms as a percentage of the assessed load at the peak load.

shear spans. Similar observation can be seen when the north shear span of CCR4 is compared with CCR3. Here, the loading configuration of CCR4 has resulted in the critical crack passing through four stirrups on the north shear span, while in CCR3 the critical crack passes through only three stirrups in both shear spans. This reduces the V_s in CCR3 compared to CCR4.

The V_d values are comparatively smaller than the other three shear transfer mechanisms but account for a non-negligible amount of the shear transmitted in the members. It should be noted that for some spans, smaller axial strains can result in lower effective yield stresses of the dowel, thus increasing the maximum capacity of the dowels, which can increase the amount of dowel action transmitted for a given vertical displacement, see Eqs. (11–13). A combination of these factors contributed to the higher dowel actions observed in CCR1 compared to other shear spans in the series.

The shear transfer mechanisms in the north and south shear spans at the peak load are shown in Fig. 14 as a percentage of the total assessed load. The percentage contribution of the CLZ toward the total shear transfer varies between 20 % and 71 %. In a previous study, it was observed that the CLZ contributes 22 %−66 % of the total shear transfer for similar members [3]. The percentage contribution of aggregate interlock for shear transfer varies between 2 % and 22 %. This is consistent with the 10 %−24 % shear transfer by aggregate interlock observed in [3]. Transverse reinforcement transfers between 21 %−54 % of total shear. This amount of shear transfer is relatively large in comparison to the total shear carried. It should be noted that large shears could be transmitted across the critical cracks in the transverse reinforcement, even though the quantity of shear reinforcement used (0.141 %) is less than the minimum reinforcement required by the CSA A23.3–19 [23], ACI 318–19 [13] and AASHTO LRFD 9th Edition [24] codes provisions for disturbed regions in most scenarios: 0.20 %, 0.25 % and 0.30 %, respectively. Similar results were observed in [3], where transverse reinforcement contributed to 21–46 % of the shear transfer. These findings indicate that in some scenarios, the transverse reinforcement can be accounted for, even if the member includes less than the minimum. The percentage contribution of dowel action is small and at the peak load, it varies between 1 % and 5 % for the 12 shear spans. Palipana et al. (2022) also observed that dowel action contributes between 2 % and 7 % of shear transfer [3].

These analyses provide a better understanding of the shear transfer mechanisms of the members and the results show that the percentage contribution of shear transfer at the peak load varies between specimens as well as between shear spans in the same specimen. Overall, the results presented are consistent with those presented by Palipana et al. (2022), where the framework gave a mean applied-to-assessed ratio of 1.09 and a coefficient-of-variation of 13.2 % for 9 shear spans examined [3]. Overall, the results are also consistent with findings in the literature for the quantification of shear transfer mechanisms in slender members [7]. This indicates that the quantification framework for deep beams, used in this manuscript, can reliably quantify the shear transfer mechanisms for a variety of specimens. Additionally, the results indicate that the quantification framework can be used with a variety of different types of displacement field measurements along the critical crack. Thus, the results support further exploring how the quantification framework can be applied in field applications to conduct crack-based assessments of structures.

4.1. *Quantification of shear transfer mechanisms throughout loading*

The methodology developed and proposed can be used to quantify the shear transfer mechanisms not only at the peak load but throughout loading. Determining the shear transfer mechanisms throughout loading can provide a better understanding of how load is shared in the different mechanisms throughout the nonlinear response.

The quantification of shear transfer mechanisms becomes more complex if the critical shear crack is not fully developed. Therefore, this section examines the shear transfer mechanisms beginning when the critical shear crack is fully formed. Fig. 15 shows the variation of the four shear transfer mechanisms, the total assessed shear force, and the applied shear force in the north and south shear spans with the deflection on the flexural tension side of the beam at a section under the load. The comparison of the assessed shear force (black) with the applied shear force (grey) shows that the approach to quantify shear transfer mechanisms proposed in this paper can capture the shear transfer mechanisms throughout loading well. The figure also demonstrates the ability to quantify the stiffness of the shear force versus displacement

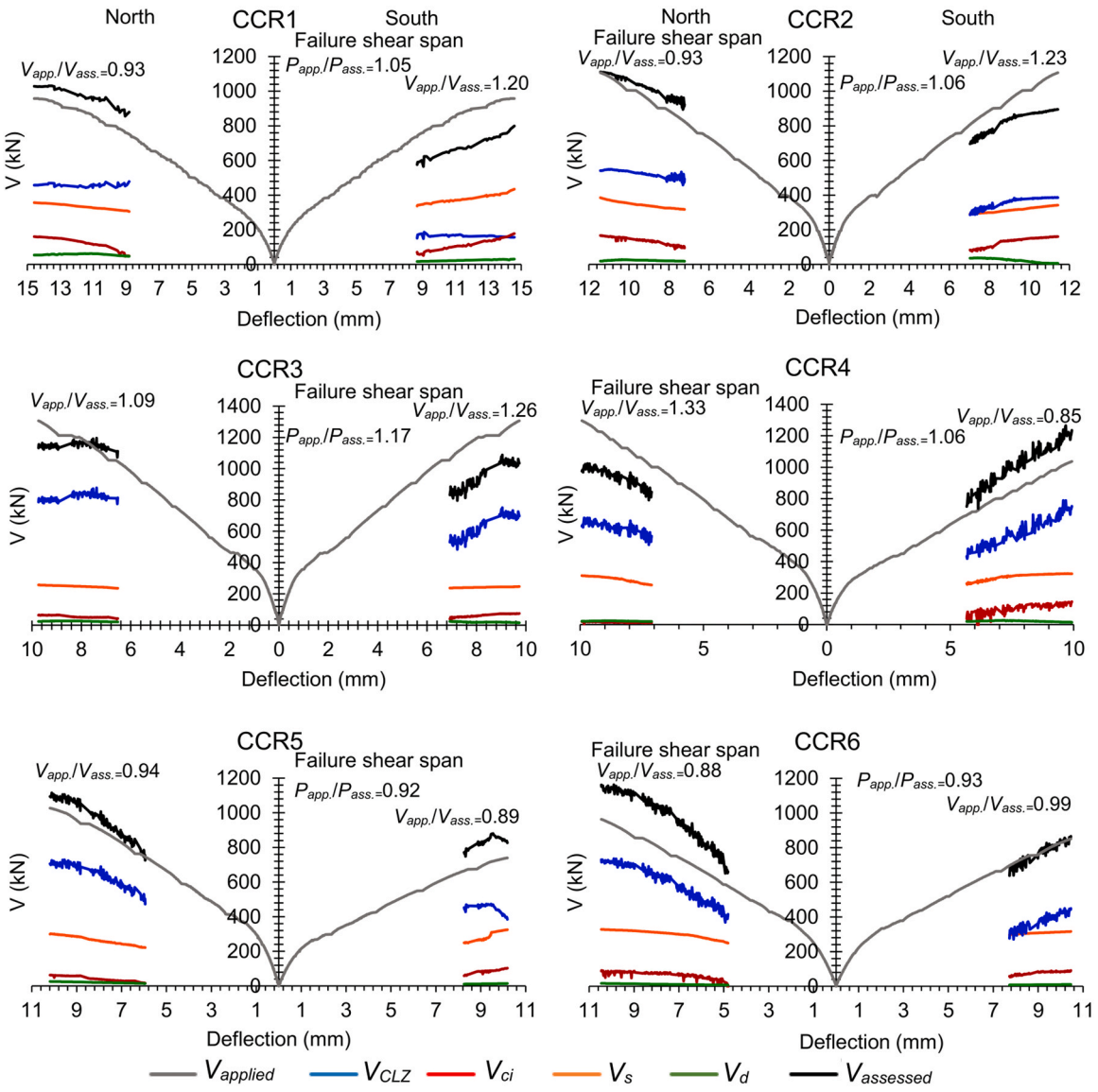

Fig. 15. Variation of shear transfer mechanisms, assessed shear force, and applied shear force in north and south shear spans with the deflection.

response well.

Except for the south shear span of CCR1, the critical loading zone (blue) has the largest contribution throughout loading. The second largest contribution for shear transfer is provided by the transverse reinforcement (orange). For most specimens, the increase in V_s observed for increasing displacements corresponds to strain-hardening which is accounted for in the quantification. Except on the north shear span of CCR4, aggregate interlock (red) transfers more shear than dowel action (green). The plots show that, with the increase of load, aggregate interlock increases. The amount of shear transferred by dowel action remains small throughout loading. In the south shear span of CCR2, the reduction of dowel action as the load increases is due to the reduction of dowel strength as the longitudinal reinforcement yields locally over the dowel length considered.

The critical loading zone in both shear spans of CCR1 and CCR2, and the north shear span of CCR3 reaches a maximum capacity when the specimen reaches a maximum shear capacity. In all other shear spans, except the south shear span of CCR5, V_{CLZ} increases with increasing shear force. In the south shear span of CCR5, V_{CLZ} begins to decrease indicating failure in the CLZ. The other shear transfer mechanisms increase to accommodate the reduction. This is particularly evident in V_s with rapid increases to accommodate the reduction in load transfer in the CLZ. In CCR6, with the increasing shear force, V_{ci}, V_s and V_d remains approximately constant. With the increase of shear force, V_{CLZ} increases proportionally. Capturing these complexities and redistribution is novel and demonstrates the capabilities of the shear quantification method presented in this paper.

5. Conclusions

This paper presents an approach to quantify shear transfer mechanisms from detailed displacement field data in shear critical reinforced concrete deep beams throughout loading. Experimental data from six large-scale deep beams monitored with full field-of-view Digital Image Correlation (DIC) equipment are studied. The four shear transfer mechanisms quantified are the shear transmitted in the critical loading zone (V_{CLZ}), by aggregate interlock (V_{ci}), by the transverse reinforcement (V_s), and by dowel action (V_d). The results provide insight into how deep beams transmit shear and can be used to inform the development of crack-based approaches and improved mechanical models of crack interfaces.

To determine the contribution of the critical loading zone, the principal strains along a vertical section at the edge of the loading plate are used in conjunction with the Modified Popovics constitutive model

to determine the stresses in the critical loading zone. Biaxial stress states in the concrete are accounted for using the Kupfer biaxial failure criterion. These stresses are integrated to determine the shear transmitted in the critical loading zone, V_{CLZ}. The critical shear cracks were automatically discretized into line segments approximately the length of the maximum coarse aggregate size, using the ACDM tool. For each crack segment along the critical crack, crack widths and crack slips were calculated. These crack kinematics were used in conjunction with the Modified CDM aggregate interlock model to obtain the shear transmitted along the critical crack, V_{ci}. The amount of shear transmitted by the transverse reinforcement across the critical crack was calculated by using the DIC data to determine the strains in the transverse reinforcement. The total shear transmitted across the critical crack, V_s, was determined by summing the forces in transverse reinforcement crossing the critical crack. Dowel deformations along longitudinal reinforcement are used to determine the dowel deformations. The dowel length, axial deformations, and dowel deformations were determined from the DIC data. The total dowel contribution for each reinforcing bar in the flexural tension region was summed to determine the total dowel action contribution, V_d.

The four quantified shear transfer mechanisms for each shear span were summed to obtain the assessed shear force, $V_{ass.}$. Comparing the assessed shear force with the experimentally measured shear force ($V_{app.}$) gave ratios of $V_{ass.}/V_{app.}$ between 0.85 and 1.33. These results gave an average $V_{ass.}/V_{app.}$ ratio of 1.04 with a 16.4 % coefficient of variation. When the shear transfer mechanisms of both shear spans of a specimen were summed and compared with the applied load, it gave $P_{ass.}/P_{app.}$ values between 0.92 and 1.17. This resulted in an average $P_{ass.}/P_{app.}$ ratio of 1.03 with a 9.1 % coefficient of variation.

At the peak load, V_{CLZ} varied between 20 % and 71 % for the 12 shear spans. It was observed that the V_{CLZ} depends on the shear span-to-depth ratio, effective loading plate size, and the crack geometry where the critical crack enters the region near the loading plate. The percentage contribution of aggregate interlock varied between 2 % and 22 %. The results also showed complex patterns of how the aggregate interlock forces, V_{ci}, varied along a critical crack, as a result of locally changing widths, slips and crack segment angles. The contribution of the transverse reinforcement, V_s, to the total shear varied between 21 % and 54 % and was larger for longer shear spans since more reinforcement crossed the critical crack. This is significant given the members are lightly reinforced with less than the minimum required reinforcement. The calculated amount of dowel action, V_d, was small compared to the other shear transfer mechanisms for this series of experiments, between 1 % and 5 % of the total shear, however, it had a non-negligible contribution.

The paper also presented the shear transfer mechanisms quantified for increasing displacements once the critical cracks on both shear spans of specimens were fully developed. As the shear force on a shear span increased, the shear transfer by each mechanism typically increased. Some mechanisms reached their maximum capacities before the specimens reached their maximum capacities. In these scenarios the shear transfer mechanisms were observed to internally redistribute the load.

The results show that the methodology presented for the quantification of shear transfer mechanisms is capable of capturing the variation of the shear transfer mechanisms throughout loading for large-scale reinforced concrete deep beams. It is expected that this methodology will be applicable for other structural elements such as slender beams, columns and walls if sufficient displacement field data, in laboratory environments or field applications, can be obtained.

CRediT authorship contribution statement

Giorgio Talotti Proestos: Writing – review & editing, Writing – original draft, Visualization, Validation, Supervision, Project administration, Methodology, Investigation, Funding acquisition, Formal analysis, Data curation, Conceptualization. **Dhanushka K. Palipana:** Writing – original draft, Validation, Methodology, Investigation, Formal analysis. **Alexandru N. Trandafir:** Writing – review & editing, Validation, Investigation, Formal analysis. **Boyan I. Mihaylov:** Writing – review & editing, Validation, Methodology, Investigation, Conceptualization.

Declaration of Competing Interest

The authors declare that they have no known competing financial interests or personal relationships that could have appeared to influence the work reported in this paper.

Data availability

Data will be made available on request.

Acknowledgements

The research was conducted by the authors as a part of an ongoing international collaborative effort on the Crack-Based Assessment of Concrete Structures (CBACS).

References

[1] Spencer BF, Hoskere V, Narazaki Y. Advances in computer vision-based civil infrastructure inspections and monitoring. Engineering 2019;5(2):199–222. https://doi.org/10.1016/j.eng.2018.11.030.
[2] Su T. Application of computer vision to crack detection of concrete structure. IACSIT Int J Eng Technol 2013;5(4):457–61. https://doi.org/10.7763/IJET.2013.V5.596.
[3] Palipana DK, Trandafir AN, Mihaylov BI, Proestos GT. Framework for the quantification of shear transfer mechanisms from deep beam experiments. Acids Struct J 2022;119(3):53–65. https://doi.org/10.14359/51734485.
[4] Trandafir AN, Palipana DK, Proestos GT, Mihaylov BI. Framework for crack based-assessment of existing lightly-reinforced concrete deep beams. Acids Struct J 2022;119(1):255–66. https://doi.org/10.14359/51733143.
[5] Trandafir AN, Proestos GT, Mihaylov BI. Detailed crack-based assessment of a 4-m deep beam test specimen. Struct Concr 2022;24(1):756–70. https://doi.org/10.1002/suco.202200149.
[6] Fan W, Chen Y, Li J, Sun Y, Feng J, Hassanin H, Sareh P. Machine learning applied to the design and inspection of reinforced concrete bridges: Resilient methods and emerging applications. Structures 2021;33(10):3954–63. https://doi.org/10.1016/j.istruc.2021.06.110.
[7] Cavagnis F, Fernández Ruiz M, Muttoni A. An analysis of the shear-transfer actions in reinforced concrete members without transverse reinforcement based on refined experimental measurements. Struct Concr 2017;19(1):1–16. https://doi.org/10.1002/suco.201700145.
[8] Mihaylov BI, Bentz EC, Collins MP. Two-parameter kinematic theory for shear behavior of deep beams. Acids Struct J 2013;110(3):447–55.
[9] Palipana DK. Assessment of Shear Transfer Mechanisms in reinforced Concrete Deep Beams from Experiments with Full Field-of-view Displacement Field Data (Ph.D. Thesis). North Carolina State University; 2023. p. 440 (Ph.D. Thesis).
[10] Palipana D.K., Proestos G.T. Large-Scale Shear Critical Reinforced Concrete Deep Beam Experiments Monitored with Full Field of View Digital Image Correlation Equipment. 26th International Conference on Structural Mechanics in Reactor Technology (SMiRT-26), Berlin/Potsdam, Germany, 2022.
[11] Palipana D.K., Proestos G.T. Asymmetrical loading of reinforced concrete deep beams monitored with full field-of-view digital image correlation. Proceedings of the 14th fib PhD Symposium in Civil Engineering, Rome, Italy, 2022.
[12] Palipana DK, Proestos GT. Behavior of shear critical concrete deep beams monitored with digital image correlation equipment. Acids Struct J 2024;121(2):181–92. https://doi.org/10.14359/51740253.
[13] ACI Committee 318. Building Code Requirements for Structural Concrete (ACI 318-19) and Commentary. Farmington Hills, MI: American Concrete Institute; 2019. p. 623.
[14] Gehri N, Mata-Falcón J, Kaufmann W. Automated crack detection and measurement based on digital image correlation. Constr Build Mater 2020;256. https://doi.org/10.1016/j.conbuildmat.2020.119383.
[15] Collins MP, Mitchell D. Prestressed Concrete Structures. Canada: Response Publication; 1997.
[16] Popovics S. A review of stress-strain relationships for concrete. Acids J 1970;67(3):243–8.
[17] Thorenfeldt E., Tomaszewicz A., Jensen J.J. Mechanical properties of high-strength concrete and application in design. Proceedings of the Symposium "Utilization of High Strength Concrete," Stavanger, Norway, June 1987, Tapir, Trondheim; 149–159.
[18] Kupfer H, Hilsdorf HK, Rusch H. Behavior of concrete under biaxial stresses. Acids J Proc 1969;66(8):656–66.

[19] Walraven JC. Fundamental analysis of aggregate interlock. J Struct Div 1981;107 (11):2245–70.
[20] Calvi PM, Bentz EC, Collins MP. Pure mechanics crack model for shear stress transfer in cracked reinforced concrete. Acids Struct J 2017;114(2):545–54. https://doi.org/10.14359/51689460.
[21] Guidotti R. Poinçonnement des planchers-dalles avec colonnes super-posées fortement sollicitées, Ph.D. thesis, Thesis no. 4812 [in French]. Leausanne, Switzerland: Ecole Polytechnique Fédérale de Lausanne; 2010. p. 446.
[22] Maekawa K, Pimanmas A, Okamura H. Nonlinear Mechanics of Reinforced Concrete. London: Spon Press; 2003.
[23] CSA Committee A23.3-19. Design of Concrete Structures. Mississauga, ON, Canada: Canadian Standards Association; 2019. p. 295.
[24] AASHTO. AASHTO LRFD Bridge Design Specifications and Commentary. ninth edition.,. Washington, DC: American Association of State Highway and Transportation Officials; 2020. p. 1912.